Eighth International Conference on
THIN-WALLED STRUCTURES- ICTWS 2018
Lisbon, Portugal, July 24-27, 2018

COUPLING BETWEEN SHELL AND GENERALIZED BEAM THEORY (GBT) ELEMENTS

Marcelo J. Bianco[1], Carsten Könke[1], Abinet Habtemariam[1] and Volkmar Zabel[1]

[1] Institute of Structural Mechanics - Bauhaus-Universität Weimar
e-mails: marcelo.jose.bianco@uni-weimar.de, carsten.koenke@uni-weimar.de,
abinet.habtemariam@uni-weimar.de, volkmar.zabel@uni-weimar.de

Keywords: Generalized Beam Theory; Coupling equations; Connections; mixed GBT-Shell model; Multi-Freedom Constraints

Abstract. *This paper presents a procedure to couple shell and Generalized Beam Theory, GBT, elements. The main focus of this procedure is the possibility to model mixed beam frame structures, which the traditional shell elements are applied at the joints and GBT elements are used to model the beams/columns. Such modeling technique can use the benefits of both elements. At the joints, shell elements can easily simulate different types of geometry conditions and details, such as stiffeners and holes; meanwhile, for the beams and columns, GBT can provide high performance, accuracy and an easy modeling approach with clear results. The numerical formulation is based on multi-freedom constrains techniques. A special attention is attributed to Master-Slaver method, which is developed based on GBT kinematic assumptions. Furthermore, there is a discussion concerning the choice of master degrees of freedom and its implications in numerical performance and the quality of model response. Finally, a detailed example of a thin-walled hollow circular cross-section is presented and its final results are compared with a full shell element model.*

1. INTRODUCTION

Generalized Beam Theory, GBT, is a numerical approach, which was initially developed to describe open thin-walled beams by Richard Schardt in Darmstadt, Germany. This approach is applicable in linear analysis [1], but it has been further extended to geometric non-linear analysis [2–4]. As an introductory point, this theory can be understood as a generalization of Vlasov Beam Theory [5]. Beyond that, GBT has a wider range of analysis, which involves distortion and shear deformation, [6–8]. In fact, GBT uses concepts of separation of variables to create i) generalized cross-section properties, which are based on shell theory; ii) a spatially-dependent longitudinal beam function. As a result, this approach presents an astonishing numerical performance and a clear representation of the displacement and stress fields as a linear combination of the generalized cross-section properties and internal forces.

However, the majority of studies and applications of GBT are limited to a single beam model. Since many structures are composed by beam frames, it is necessary to handle the interaction among beams that share a common node. Here, it stands out two obstacles. The first one is due to complexity in the kinematic coupling among the GBT's deformation shapes at the connection node, which involves several modes simultaneously. The next section presents the bibliographic review and the state-of-art about this issue. The second obstacle is concerning the physical connection itself. In practical structural design, substantial amount of details rise at the

connection, such as stiffeners, bolts and weldings for steel structures. These details not only change the kinematic behavior of the connection, but they are infeasible to be modeled in as beam element.

Thus, due to a high level of detailing in structural connections, shell and solid elements are widely applied in their structural analysis. Therefore, it is convenient to split the structural analysis into two domains: the first is the beam domain, in which GBT elements are applied; the second one is the connection domains, in which shell or solid elements are used.

This domain separation leads directly to the question of how to couple the degrees of freedom of shell and solid elements with the high order of GBT's degrees of freedom, which represent the modal deformation.

The current study develops a novel application of Multi-Freedom Constraints in a coupling method between shell and GBT elements, in order to solve the question of the previous paragraph. Also, it provides a detailed numerical example to illustrate the proposed method, as well as to compare the result of the mixed GBT-shell models with pure shell models.

2. PURE GBT BEAM FRAME ANALYSIS

The expression used here, pure GBT beam frame analysis, is the nomenclature to describe numerical models which only involve GBT's finite elements.

The first studies in this application were not directly related to GBT, but they were concerning warping transmission of Vlasov beam element [9], [10] and [11], which can be understood as the first high mode of GBT.

Basaglia et al., [12] and [13], are the first ones to study the warping as a high mode of GBT. They highlight not only the main role of the layout of connection in warping transmission, but also identify and classify extra kinematic behavior of connection in high modes: internal support (no internal force and deformation transmission) and the inversed-clamped (totally inverse transmission of internal forces and deformation).

To clarify how the connection layout affects the hight modes transmission, one can consider four particular types of connections between beams with "I" profile: non-stiffener, box, diagonal, and box-diagonal connections:

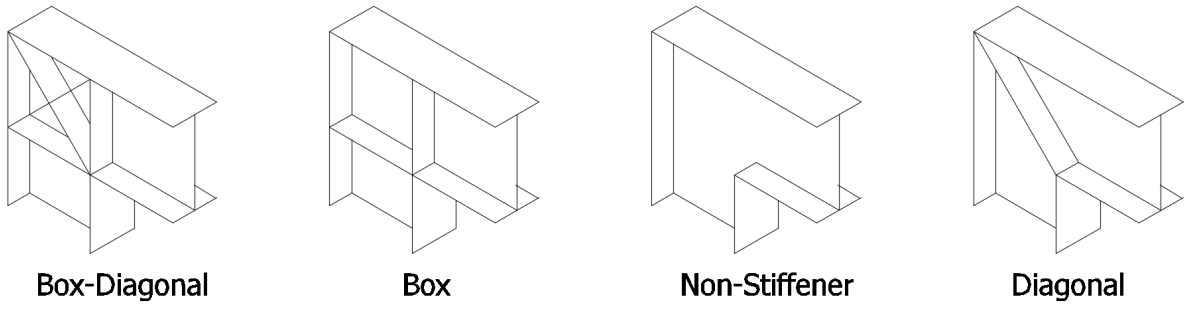

Figure 1: Type of connections to clarify the kinematic behavior in high modes

Box-Diagonal: The first connection in figure 1 leads to internal support behavior, which is nothing less than the restrain of a cross-section warping and/or distortion by stiffeners. Since all internal forces beyond of the traditional six degrees of freedom have two or more opposite forces/bending moments in the cross-section, a stiffener component can directly link these opposite forces/bending moments, which will annul them.

Box: The second connection in figure 1 is an example of how it is possible to transmit inverse internal forces of high modes. Figure 2.a shows how the bi-moment can be decomposed in flanges' bending moments. These bending moments, in their turn, are supported by the reaction forces in the stiffeners. These reactions act in the column's flanges as concentrated bending moments, similar to the case of the beam's flanges. However, these local bending moments in the column have an opposite direction when compared to the local bending moments in the flange of the beam. Therefore, an inverse internal force transmission mechanism is built.

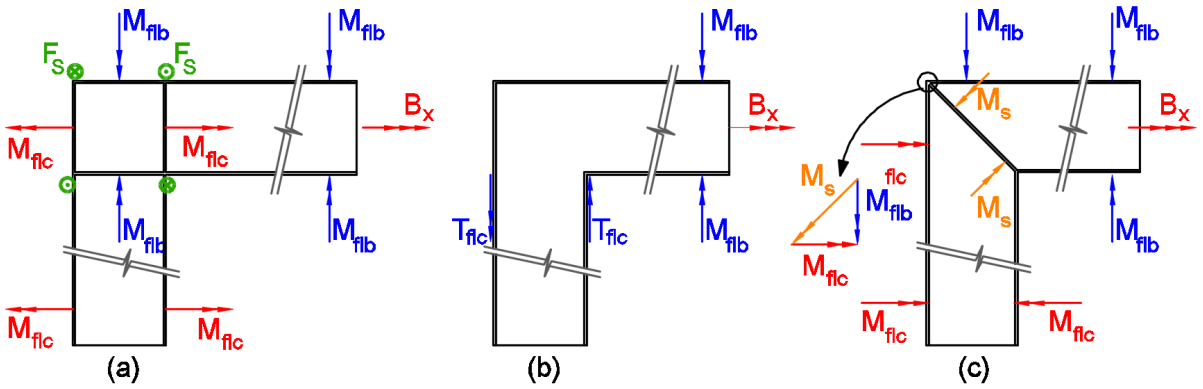

Figure 2: Kinematic mechanism and equilibrium of connection; a) box with inversed transmission; b) Non-Stiffener, which leads to transmission between warping and distortion; c) Diagonal stiffener with directly transmission.

Non-Stiffener: The third connection in figure 1 explains not only a hinge behavior of GBT's high modes, but also it is a good example how these modes can be coupled due to connection. Similar to the explanation of box connection, figure 2.b shows how the bi-moment is transmitted among the flanges of columns and beams. However, in this case, instead of a reaction binary force in vertical stiffener, the restraint is provided by the torsional inertia of each individual column's flange and the flexural bending stiffness of the web. Therefore, the warping in beam is transformed it column's distortion. In fact, there is a residual bi-moment inversed transmission between the beam and column, due to web stiffness. Nevertheless, the web's capacity for warping transmission is quite limited, specially in thin-walled structures.

Diagonal: The last connection in figure 1 has a direct transmission of internal forces and displacements, which can be understood as clamped behavior. Differently from the box connections, the local bending moments of the beam's flanges in the diagonal ones are not balanced by binary forces due to the reactions of the stiffeners. Instead, they are balanced by the moments' equilibrium at points of intersection among i) the flanges of the column; ii) the flange of the beam; and iii) the diagonal stiffener, as presented in figure 2.c.

However, this simple explanation has the assumption of null torsional inertia in the stiffener and flanges. If the connection has thick stiffener and flanges, then the torsion inertia in these components will restrain the connection to warping. Consequently, this connection has a partial behavior of box-diagonal connection, which limits the fully warping and bi-moment transmission.

3. CONNECTIONS OBTAINED FROM COUPLING BETWEEN GBT AND SHELL ELEMENTS

From the examples of warping transmission in the previous section, it becomes clear that the connections involving GBT's high modes are not only complex concerning about the kinematic mechanism, but also about the unique properties of these modes. Besides that, a usual structure

connection involves many details, such as welds, bolts, holes, stiffeners etc, which require a minute modeling and analysis, usually carried on by shell or solid finite elements.

Since the main field of application of GBT is thin-walled structures and the connections of these structures are often modeled by shell elements, the focus of this section is in the coupling between these elements and GBT elements.

The coupling approach proposed here is a novel application of multi-freedom constraint based on Master-Slave method for beam frames and connections [14, 15]. It uses the superposition property of GBT's deformation modes to setup the relationship between the master and slavers degrees of freedom. Furthermore, these degrees of freedom are divided in two groups: shell and GBT. Each group is related to a master or slaver degree of freedom and different of traditional applications. The presented approach predefines which group is the master and which is the slaver. These details are discussed in the sequence.

3.1. Definition of master and slaver degrees of freedom

Usually, in Master-Slaver multi-freedom constraintmethod, there is no rule in the definition of which degree of freedom is the master and which one is the slaver. However, in the present implementation, this definition is predefined. Since the main focus of the proposed procedure is to build up a degree of freedom's mapping of type shell-GBT or GBT-shell, and avoiding any type of restrain of type GBT-GBT or shell-shell, one can classify the degree of freedom as shell or GBT group. Once this limitation and classification are defined, the next issue is which group is the master, and which is the slaver.

The direct answer of this question is: the degrees of freedom of GBT are the master ones.

This choice is not arbitrary. It is based on the fact that one GBT node has a lower amount of degrees of freedom than the summation of all degrees of freedom of shell elements used to described a cross-section. For instance, one can consider the coupling of a hollow circular cross-section, as plotted in figure 3. This coupling cross-section has 28 shell nodes, each node has 6 degrees of freedom, in a total of 168 degrees of freedom. This same cross-section can be described in GBT by 6 deformation modes, having each one two degrees of freedom per node (there are few exceptions, such as the uniform torsion or the uniform longitudinal elongation deformation modes, which requires just one degree of freedom per node). Consequently, GBT requires a total of 12 degrees of freedom.

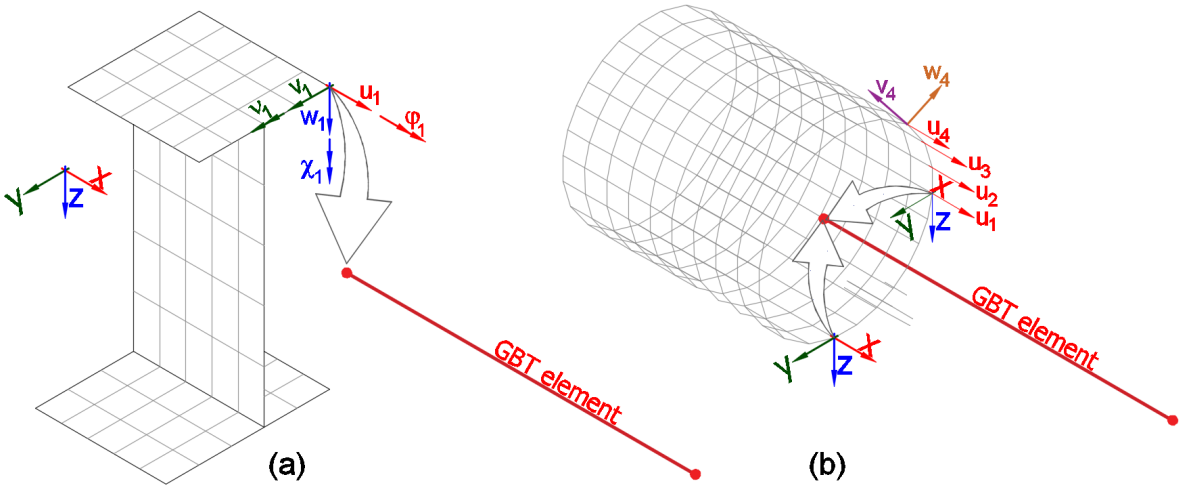

Figure 3: Orientation of degrees of freedom in coupling between shell and GBT's elements: a) generic segmented cross-section b)hollow circular cross-section

Since the finite element model's response is always limited by the coarse description of the cross-section, the opposite choice, shell's degrees of freedom as master ones, is numerical inefficient. This alternative definition requires only more computer effort to reach the results of the choice mentioned on the previous paragraph.

3.2. Master-Slaver relationships based on GBT's deformation modes

The coupling between shell and GBT's degrees of freedom can be expressed in matrix form as:

$$[\vartheta]_{shell} = [T_c]\,[\vartheta]_{GBT} \tag{1}$$

Where, $[\vartheta]_{shell}$ and $[\vartheta]_{GBT}$ are the displacement vectors of shell and GBT's degrees of freedom, respectively; and $[T_c]$ is the multi-freedom constrainttransformation matrix, which is based on GBT's description of displacement field as a summation of the modal displacement:

$$u(x,s) = \sum_{i=1}^{n} {}^{i}u(s)\,{}^{i}V_{,x}(x) \quad (2)\;\; v(x,s) = \sum_{i=1}^{n} {}^{i}v(s)\,{}^{i}V(x) \quad (3)\;\; w(x,s) = \sum_{i=1}^{n} {}^{i}w(s)\,{}^{i}V(x) \quad (4)$$

Here, u, v and w are the displacement in longitudinal, transversal tangential and transversal perpendicular directions respectively, as shown in figure 3; V is the amplification function of these displacements along the beam length; and the upper-left index i indicates the GBT's deformation mode. Hence, these equations are used to express the shell's nodal displacement. For instance, the longitudinal displacement of node 1, in shell element discretization shown in figure 3, can be expressed as:

$$u_{1,shell} = \sum_{i=1}^{m} {}^{i}u(s)\,{}^{i}V_{,x}(x = -L/2) \tag{5}$$

Where, the longitudinal position in beam element, x, is set at one of the extreme nodes: $x = -L/2$ or $x = L/2$ (in a centered-origin element). This summation can be represented in a matrix form, which is already the main component of multi-freedom constraint transformation matrix:

$$[u]_{shell} = [T_c]_u\,[V_{,x}]_{GBT}\,; \qquad \begin{bmatrix} u_1 \\ u_2 \\ u_3 \\ u_4 \\ \vdots \\ u_n \end{bmatrix}_{shell} = \begin{bmatrix} {}^{1}u_1 & {}^{2}u_1 & {}^{3}u_1 & \dots & {}^{m}u_1 \\ {}^{1}u_2 & {}^{2}u_2 & {}^{3}u_2 & \dots & {}^{m}u_2 \\ {}^{1}u_3 & {}^{2}u_3 & {}^{3}u_3 & \dots & {}^{m}u_3 \\ {}^{1}u_4 & {}^{2}u_4 & {}^{3}u_4 & \dots & {}^{m}u_4 \\ \vdots & \vdots & \vdots & \ddots & \vdots \\ {}^{1}u_n & {}^{2}u_n & {}^{3}u_n & \dots & {}^{m}u_n \end{bmatrix} \begin{bmatrix} {}^{1}V \\ {}^{2}V_{,x} \\ {}^{3}V_{,x} \\ \vdots \\ {}^{m}V_{,x} \end{bmatrix}_{GBT} \tag{6}$$

Here, the indexes n and m indicate the number of shell node and GBT's modes, respectively.

It is not necessary that the shell nodes and the GBT cross-section discretization nodes are in the same geometric position. The only restriction is the imposition of shell nodes to be in the middle line of the cross-section discretization. Since this condition is maintained, an arbitrary shell node position can be coupled with GBT modes by the interpolation functions of the cross-section segment. For instance, a linear interpolation function of u, in a centered-origin segment of a cross-section, can be expressed by:

$${}^{i}u_h(s) = \begin{bmatrix} s & 1 \end{bmatrix} \frac{1}{2l_s} \begin{bmatrix} -2 & 2 \\ l_s & l_s \end{bmatrix}^{i} \begin{bmatrix} u_1 \\ u_2 \end{bmatrix} = [Ts_{He1}]\,[Sh_{He1cc}]\,{}^{i}[u_h] \tag{7}$$

Where s is the position in cross-section segment and l_s is the total segment length. The intro-

duction of this expression in eq. 6 leads to:

$$\begin{bmatrix} u_1 \\ u_2 \\ u_3 \\ u_4 \\ \vdots \\ u_n \end{bmatrix}_{shell} = [TS1]_{seg}\,[u_h]_{seg} \begin{bmatrix} {}^1V \\ {}^2V_{,x} \\ {}^3V_{,x} \\ \vdots \\ {}^nV_{,x} \end{bmatrix}_{GBT} \tag{8}$$

Here, $[TS1]_{seg}$ is a matrix, which the number of rows is the number of shell nodes and the number of columns is the number of segments of the cross-section that contains the shell nodes. This matrix is populated in each row by the linear Hermitian interpolation function of $[Ts_{He1}]\,[Sh_{He1cc}]$, in the respective column of the segment, which has the shell node. For example, in a hypothetic application, the shell nodes 1 is in cross-section segment 1, shell nodes 2 and 3 are in segment 2 and shell node 4 is segment 3. For this case, one obtains the following interpolation segment matrix:

$$[TS1]_{seg} = \begin{bmatrix} [Ts_{He1}]_{s1}\,[Sh_{He1cc}]_{s1} & 0 & 0 & \dots \\ 0 & [Ts_{He1}]_{s2}\,[Sh_{He1cc}]_{s2} & 0 & \dots \\ 0 & [Ts_{He1}]_{s2}\,[Sh_{He1cc}]_{s2} & 0 & \dots \\ 0 & 0 & [Ts_{He1}]_{s3}\,[Sh_{He1cc}]_{s3} & \dots \\ \vdots & \vdots & \vdots & \ddots \end{bmatrix} \tag{9}$$

Where the lower-right indexes $s1$, $s2$ and $s3$ indicate the relative cross-section segment. The second matrix in right-hand side of eq. 8, $[u_h]_{seg}$, is nothing less that all modal longitudinal displacement of each segment, which has shell nodes:

$$[u_h]_{seg} = \begin{bmatrix} {}^1[u_h]_{s1} & {}^2[u_h]_{s1} & {}^3[u_h]_{s1} & \dots & {}^m[u_h]_{s1} \\ {}^1[u_h]_{s2} & {}^2[u_h]_{s2} & {}^3[u_h]_{s2} & \dots & {}^m[u_h]_{s2} \\ {}^1[u_h]_{s3} & {}^2[u_h]_{s3} & {}^3[u_h]_{s3} & \dots & {}^m[u_h]_{s3} \\ \vdots & \vdots & \vdots & \ddots & \vdots \end{bmatrix} \tag{10}$$

The transversal displacement v and w are obtained in a similar way. The only change is the absence of mode 1. If the shell nodes share the same position of GBT nodes of cross-section discretization, one finds:

$$[v]_{shell} = [T_c]_v\,[V]_{GBT}\,; \qquad \begin{bmatrix} v_1 \\ v_2 \\ v_3 \\ \vdots \\ v_n \end{bmatrix}_{shell} = \begin{bmatrix} {}^2v_1 & {}^3v_1 & {}^4v_1 & \dots & {}^nv_1 \\ {}^2v_2 & {}^3v_2 & {}^4v_2 & \dots & {}^nv_2 \\ {}^2v_3 & {}^3v_3 & {}^4v_3 & \dots & {}^nv_3 \\ \vdots & \vdots & \vdots & \ddots & \vdots \\ {}^2v_6 & {}^3v_6 & {}^4v_6 & \dots & {}^nv_6 \end{bmatrix} \begin{bmatrix} {}^2V \\ {}^3V \\ {}^4V \\ \vdots \\ {}^nV_{,x} \end{bmatrix}_{GBT} \tag{11}$$

$$[w]_{shell} = [T_c]_w\,[V]_{GBT}\,; \qquad \begin{bmatrix} w_1 \\ w_2 \\ w_3 \\ \vdots \\ w_n \end{bmatrix}_{shell} = \begin{bmatrix} {}^2w_1 & {}^3w_1 & {}^4w_1 & \dots & {}^nw_1 \\ {}^2w_2 & {}^3w_2 & {}^4w_2 & \dots & {}^nw_2 \\ {}^2w_3 & {}^3w_3 & {}^4w_3 & \dots & {}^nw_3 \\ \vdots & \vdots & \vdots & \ddots & \vdots \\ {}^2w_6 & {}^3w_6 & {}^4w_6 & \dots & {}^nw_6 \end{bmatrix} \begin{bmatrix} {}^2V \\ {}^3V \\ {}^4V \\ \vdots \\ {}^nV \end{bmatrix}_{GBT} \tag{12}$$

Else, the shell nodes are in another point of the cross-section segments. It is necessary to apply

the interpolation functions of respective displacement, which leads to:

$$\begin{bmatrix} v_1 \\ v_2 \\ v_3 \\ v_4 \\ \vdots \\ v_n \end{bmatrix}_{shell} = [TS1]_{seg}\,[v_h]_{seg} \begin{bmatrix} {}^2V \\ {}^3V \\ {}^4V \\ \vdots \\ {}^nV \end{bmatrix}_{GBT} \quad (13) \qquad \begin{bmatrix} w_1 \\ w_2 \\ w_3 \\ w_4 \\ \vdots \\ w_n \end{bmatrix}_{shell} = [TS3]_{seg}\,[w_h]_{seg} \begin{bmatrix} {}^2V \\ {}^3V \\ {}^4V \\ \vdots \\ {}^nV \end{bmatrix}_{GBT} \quad (14)$$

Where, $[TS3]_{seg}$ is the cubic Hermitian interpolation function of transversal displacement w given by:

$${}^i w_h(s) = \begin{bmatrix} s^3 & s^2 & s & 1 \end{bmatrix} \frac{1}{8l_s^3} \begin{bmatrix} 16 & 8l_s & -16 & 8l_s \\ 0 & -4l_s^2 & 0 & 4l_s^2 \\ -12l_s^2 & -2l_s^3 & 12l_s^2 & -2l_s^3 \\ 4l_s^3 & l_s^4 & 4l_s^3 & -l_s^4 \end{bmatrix}^i \begin{bmatrix} w_1 \\ \phi_1 \\ w_2 \\ \phi_2 \end{bmatrix} = [Ts_{He3}][Sh_{He3cc}]^i [w_h] \quad (15)$$

The GBT modal segment matrices: $[v_h]_{seg}$ and $[w_h]_{seg}$ follow the same procedure of longitudinal displacement.

Concerning the rotational degrees of freedom, one can directly setup the coupling of transversal rotation, υ, as shown in figure 3.a, between shell elements and the generic segmented cross-section based on GBT definition of longitudinal rotation:

$$\upsilon(x,s) = \sum_{i=1}^{n} {}^i w(s)\, {}^i V_{,x}(x) \quad (16)$$

Thus, the transversal rotation coupling can be expressed by the multi-freedom constraint transformation matrix, $[T_c]_w$, and GBT's degrees of freedom of generalized rotation, $[V_{,x}]_{GBT}$, which are given in equations 12 and 6, respectively:

$$[\upsilon]_{shell} = [T_c]_w\,[V_{,x}]_{GBT} \quad (17)$$

In the more generic case, in which the shell nodes lay at an arbitrary point in the GBT segment, the coupling expression is given by:

$$\begin{bmatrix} \upsilon_1 \\ \upsilon_2 \\ \upsilon_3 \\ \upsilon_4 \\ \vdots \\ \upsilon_n \end{bmatrix}_{shell} = [TS3]_{seg}\,[w_h]_{seg} \begin{bmatrix} {}^2V_{,x} \\ {}^3V_{,x} \\ {}^4V_{,x} \\ \vdots \\ {}^nV_{,x} \end{bmatrix}_{GBT} \quad (18)$$

Following a similar procedure, one obtains the coupling of longitudinal rotation, φ, which is based on GBT's definition of longitudinal rotation:

$$\varphi(x,s) = \sum_{i=1}^{n} {}^i w_{,s}(s)\, {}^i V(x) \quad (19)$$

If GBT's discretization and shell nodes share the same position, no interpolation in GBT segment

is necessary. Thereby, one finds:

$$[\varphi]_{shell} = [T_c]_{\varphi}\,[V]_{GBT}\,; \qquad \begin{bmatrix} \varphi_1 \\ \varphi_2 \\ \varphi_3 \\ \varphi_4 \\ \vdots \\ \varphi_n \end{bmatrix}_{shell} = \begin{bmatrix} {}^2\varphi_1 & {}^3\varphi_1 & {}^4\varphi_1 & \dots & {}^n\varphi_1 \\ {}^2\varphi_2 & {}^3\varphi_2 & {}^4\varphi_2 & \dots & {}^n\varphi_2 \\ {}^2\varphi_3 & {}^3\varphi_3 & {}^4\varphi_3 & \dots & {}^n\varphi_3 \\ {}^2\varphi_4 & {}^3\varphi_4 & {}^4\varphi_4 & \dots & {}^n\varphi_4 \\ \vdots & \vdots & \vdots & \ddots & \vdots \\ {}^2\varphi_n & {}^3\varphi_n & {}^4\varphi_n & \dots & {}^n\varphi_n \end{bmatrix} \begin{bmatrix} {}^2V \\ {}^3V \\ {}^4V \\ \vdots \\ {}^nV \end{bmatrix}_{GBT} \tag{20}$$

Else, the coupling by interpolated values inside of a GBT segment can be expressed as:

$$\begin{bmatrix} \varphi_1 \\ \varphi_2 \\ \varphi_3 \\ \varphi_4 \\ \vdots \\ \varphi_n \end{bmatrix}_{shell} = [TS3_{,s}]_{seg}\,[w_h]_{seg} \begin{bmatrix} {}^2V \\ {}^3V \\ {}^4V \\ \vdots \\ {}^nV \end{bmatrix}_{GBT} \tag{21}$$

where, the subindex $_{,s}$ indicates the first derivative of interpolation segment matrix $[TS3]_{seg}$.

The transversal perpendicular rotational degree of freedom, χ, shown in figure 3.a, requires special remarks.

The first one is about the GBT's assumption of a linear variation of the longitudinal displacement in each cross-section segment. It leads to a constant transversal perpendicular rotation in each segment. Thus, if GBT's discretization and shell nodes **do not** share the same position, one can reach the following expression:

$$\begin{bmatrix} \chi_1 \\ \chi_2 \\ \chi_3 \\ \chi_4 \\ \vdots \\ \chi_n \end{bmatrix}_{shell} = [T_c]_{\chi}\,[V_{,x}]_{GBT} = [TS1_{,s}]_{seg}\,[u_h]_{seg} \begin{bmatrix} {}^1V \\ {}^2V_{,x} \\ {}^3V_{,x} \\ \vdots \\ {}^nV_{,x} \end{bmatrix}_{GBT} \tag{22}$$

However, since each segment can have a different constant value of this rotation, it leads to a discontinuity at GBT nodes of cross-section discretization. Consequently, if GBT's discretization and shell nodes share the same position, there are ambiguous values of GBT transversal perpendicular rotation to couple.

In a simple-minded approach, this problem can overcome the average among the transversal perpendicular rotation of each segment that reach the node.

The second remark is about the type of shell element used. Many shell elements don't have this degree of freedom, which is named in literature as drilled degree of freedom. For these shell elements, there is no coupling for this transversal rotation and all information about it is vanished.

3.2.1. Coupling with different global coordinate system - the hollow circular cross-section case

It is important to observe that the approach presented up to this point considers a common coordinate system between shell and GBT elements. Usually, this condition is found in generic segmented cross-section. However, for a hollow circular cross-section, under GBT's formula-

tion, the coordinate systems are not the same, such as local coordinate system presented in figure 4.b, which is left-hand. Therefore, coupling for hollow circular cross-section requires an extra transformation for this displacement v and w:

$$\begin{bmatrix} [v]_{shell} \\ [w]_{shell} \end{bmatrix}_{Scs} = \begin{bmatrix} -\sin(\theta_1) & \dots & 0 & \cos(\theta_1) & \dots & 0 \\ \vdots & \ddots & \vdots & \vdots & \ddots & \vdots \\ 0 & \dots & -\sin(\theta_n) & 0 & \dots & \cos(\theta_n) \\ \cos(\theta_1) & \dots & 0 & \sin(\theta_1) & \dots & 0 \\ \vdots & \ddots & \vdots & \vdots & \ddots & \vdots \\ 0 & \dots & \cos(\theta_n) & 0 & \dots & \sin(\theta_n) \end{bmatrix} \begin{bmatrix} [v]_{shell} \\ [w]_{shell} \end{bmatrix}_{GBTcs} \tag{23}$$

Where, θ_n is the angle of each shell node according to GBT's local coordinate system, as shown in figure 4.b; the subindexes $_{Scs}$ and $_{GBTcs}$ indicate the Shell coordinate system and the GBT's coordinate system.

The transversal rotations require the same treatment:

$$\begin{bmatrix} [v]_{shell} \\ [\chi]_{shell} \end{bmatrix}_{Scs} = \begin{bmatrix} -\sin(\theta_1) & \dots & 0 & \cos(\theta_1) & \dots & 0 \\ \vdots & \ddots & \vdots & \vdots & \ddots & \vdots \\ 0 & \dots & -\sin(\theta_n) & 0 & \dots & \cos(\theta_n) \\ \cos(\theta_1) & \dots & 0 & \sin(\theta_1) & \dots & 0 \\ \vdots & \ddots & \vdots & \vdots & \ddots & \vdots \\ 0 & \dots & \cos(\theta_n) & 0 & \dots & \sin(\theta_n) \end{bmatrix} \begin{bmatrix} [v]_{shell} \\ [\chi]_{shell} \end{bmatrix}_{GBTcs} \tag{24}$$

3.2.2. Coupled stiffness matrix and external load vector

Once the multi-freedom constraint matrices are evaluated, the next step in the mixed shell-GBT model is the setup of couped stiffness matrix and the external load vector. It is easily achieved by the respective matrices transformation:

$$[K]_{cp} = [T_c]_{tot}^T [K]_{uc} [T_c]_{tot} \tag{25}$$

$$[F]_{cp} = [T_c]_{tot}^T [F]_{uc} \tag{26}$$

where, the subindexes $_{cp}$ and $_{uc}$ indicate the coupled and uncoupled matrices, respectively. The total coupling transformation matrix, $[T_c]_{tot}$, is an identity matrix of the same rank of the uncoupled stiffness matrix, which has the columns concerning the coupled shell's degrees of freedom removed. Furthermore, the row concerning these degrees of freedom are re-populated by the values of matrices $[T_c]_u$, $[T_c]_v$, $[T_c]_w$, $[T_c]_\varphi$ and $[T_c]_\chi$. The next section shows the implementation of this matrix by a detailed example.

4. NUMERICAL EXAMPLE OF COUPLING GBT AND SHELL ELEMENTS

As a detailed numerical example of the application of coupling between Shell and GBT elements, let us consider the thin-walled circular hollow steel cross-section shown in Figure 4. This cross-section is applied in a vertical cantilever structure subjected to a linear projected surface load, i.e. the total load applied on the structure is not a product of the surface load and the area of the surface, it is the product of the surface load and the projected area on the global coordinate direction z. The material parameters are Young Modulus $E = 205,000 N/mm^2$, Poisson's ratio $\mu = 0.3$, and Shear Modulus $G = 78,846.2 N/mm^2$.

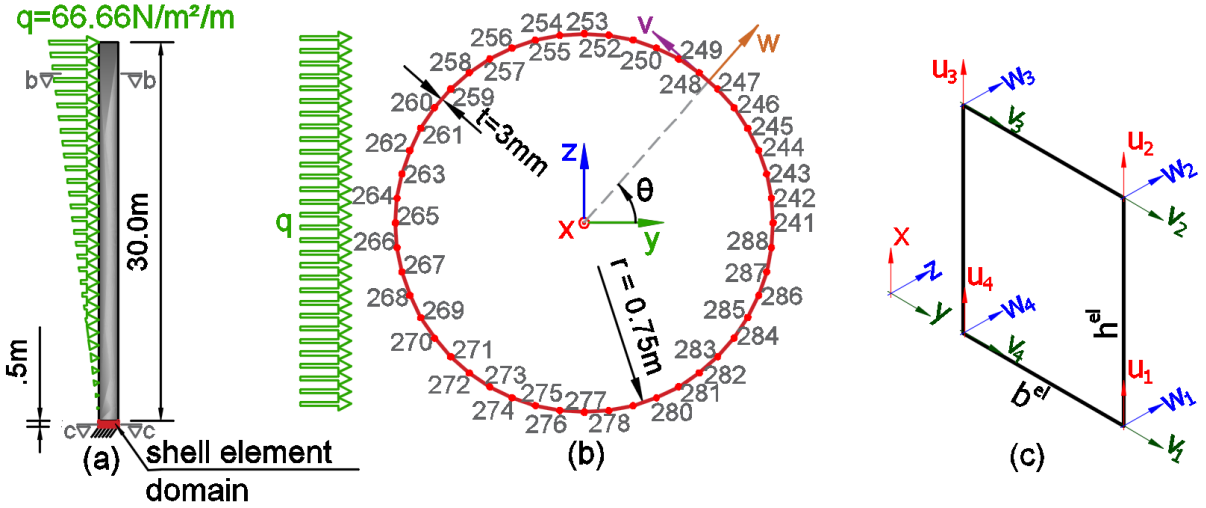

Figure 4: Thin-walled circular hollow section under a linear projected force and a coupled shell element segment; a) Elevation; b) Cross-section in GBT's domain; c) Cross-section in shell's domain at the coupling point

4.1. Setup of finite element and coupling matrices

The structure is 30.5 m high, of which the upper 30m is modeled by 1 exact GBT element [16], with 3 nodes per element, 2 degrees of freedom per node and 5 deformation modes: 1 for radial deformation (i=a); 1 for bending (i=3); and 3 for ovalization (i=5,7 and 11). The respective transversal and longitudinal displacements of these modes are provided in table. 1. Thus, there is a total of 30 GBT's degrees of freedom.

Table 1: Relevant orthogonal deformation shape modes in this example

i	m	${}^{i}u$	${}^{i}v^{\star}$	${}^{i}w$
a	0	0	0	1
3	1	$-r\cos(\theta)$	$-\sin(\theta)$	$\cos(\theta)$
5	2	$-r\cos(2\theta)$	$-2\sin(2\theta)$	$2^2\cos(2\theta)$
7	3	$-r\cos(3\theta)$	$-3\sin(3\theta)$	$3^2\cos(3\theta)$
11	5	$-r\cos(5\theta)$	$-5\sin(5\theta)$	$5^2\cos(5\theta)$

The lower half meter is discretized by shell elements, which has 48 node elements in transversal direction and 5 layers of elements in the longitudinal direction. Thus, the shell part of the model has 288 nodes and 240 shell elements. Consequently, all elements have the same proportion and shape. Moreover, they are limited to the well-known membrane behavior [17], which leads to 3 degrees of freedom per node. Therefore, a total of 864 degrees of freedom is obtained. From this total, 48 nodes (144 degrees of freedom at the base) are restrained to the displacement. The same amount will be restrained at the top cross-section of this prolongation by the multi-freedom constraint matrix. The final mixed model has 576 free degrees of freedom from shell part.

The transformation from the local (shown in figure. 4.c) to global coordinate system of each shell element and the assembly of the global stiffness matrix follows the well-known approach of FEM [17]. To this global stiffness obtained from the shell elements, the GBT stiffness matrices are added, which, this step, are still uncoupled among each other, as well as among the membrane's degrees of freedom. Table 2 resumes the setup of the degrees of freedom.

Table 2: Setup of degrees of freedom in mixed membrane-GBT model

displacement	DOF's	Support restrain	Master DOF	Slavers DOF
u	1 to 288	1 to 48	–	241 to 288
v	289 to 576	289 to 337	–	529 to 576
w	577 to 864	577 to 625	–	817 to 864
${}^{3}V$	865;867;869	–	865	–
${}^{3}V_{,x}$	866;868;870	–	866	–
${}^{5}V$	871;873;875	–	871	–
${}^{5}V_{,x}$	872;874;876	–	872	–
${}^{7}V$	877;879;881	–	877	–
${}^{7}V_{,x}$	878;880;882	–	878	–
${}^{11}V$	883;885;887	–	883	–
${}^{11}V_{,x}$	884;886;888	–	884	–
${}^{15}V$	889;891;893	–	889	–
${}^{15}V_{,x}$	890;892;894	–	890	–
${}^{a}V$	895;897;899	–	895	–
${}^{a}V_{,x}$	896;898;900	–	896	–

4.1.1. Coupling of longitudinal displacement - *u*

In order to couple the longitudinal displacement, u, one must evaluate the multi-freedom constraint transformation matrix, $[T_c]_u$, for each slaver degree of freedom with respect to each GBT mode. To do so, it is necessary to compute the modal longitudinal displacement of each slaver node, given in table 1, with the respective node angle θ, where the $\Delta\theta$ between the nodes is 7.5° as presented in figure 4.b. These results are introduced into eq. 6, leading to:

$$[T_c]_u = -750 \begin{array}{c} \\ 241 \\ 242 \\ 243 \\ 244 \\ \vdots \\ 288 \end{array} \begin{array}{c} \begin{array}{cccccc} 866 & 872 & 878 & 884 & 890 & 896 \end{array} \\ \begin{bmatrix} \cos(0°) & \cos(0°) & \cos(0°) & \cos(0°) & \cos(0°) & 0 \\ \cos(7.5°) & \cos(15°) & \cos(22.5°) & \cos(37.5°) & \cos(52.5°) & 0 \\ \cos(15°) & \cos(30°) & \cos(45°) & \cos(75°) & \cos(105°) & 0 \\ \cos(22.5°) & \cos(45°) & \cos(67.5°) & \cos(112.5°) & \cos(157.5°) & 0 \\ \vdots & \vdots & \vdots & \vdots & \vdots & \vdots \\ \cos(352.5°) & \cos(705°) & \cos(1057.5°) & \cos(1762.5°) & \cos(2467.5°) & 0 \end{bmatrix} \end{array} \tag{27}$$

On the left and on the top, the row and column indexes indicate the slave and master degrees of freedom, respectively. Since the longitudinal displacement of GBT is consistent with the global coordinate system of the membranes, no extra transformation is required for these degrees of freedom.

4.1.2. Coupling of transversal displacements - *v* and *w*

Similar to the coupling of longitudinal displacement, the transversal coupling is obtained by the multi-freedom constraint transformation matrices $[T_c]_v$ and $[T_c]_w$, which are based on the

expression of table 1. Therefore, one can find:

$$[T_c]_v = -1$$

$$\begin{array}{c} \\ 529 \\ 530 \\ 531 \\ 532 \\ \vdots \\ 576 \end{array} \begin{array}{c} \begin{array}{cccccc} 865 & 871 & 877 & 883 & 889 & 895 \end{array} \\ \begin{bmatrix} \sin(0°) & 2\sin(0°) & 3\sin(0°) & 5\sin(0°) & 7\sin(0°) & 0 \\ \sin(7.5°) & 2\sin(15°) & 3\sin(22.5°) & 5\sin(37.5°) & 7\sin(52.5°) & 0 \\ \sin(15°) & 2\sin(30°) & 3\sin(45°) & 5\sin(75°) & 7\sin(105°) & 0 \\ \sin(22.5°) & 2\sin(45°) & 3\sin(67.5°) & 5\sin(112.5°) & 7\sin(157.5°) & 0 \\ \vdots & \vdots & \vdots & \vdots & \vdots & \vdots \\ \sin(352.5°) & 2\sin(705°) & 3\sin(1057.5°) & 5\sin(1762.5°) & 7\sin(2467.5°) & 0 \end{bmatrix} \end{array} \tag{28}$$

$$[T_c]_w =$$

$$\begin{array}{c} \\ 817 \\ 818 \\ 819 \\ 820 \\ \vdots \\ 864 \end{array} \begin{array}{c} \begin{array}{cccccc} 865 & 871 & 877 & 883 & 889 & 895 \end{array} \\ \begin{bmatrix} \cos(0°) & 4\cos(0°) & 9\cos(0°) & 25\cos(0°) & 49\cos(0°) & 1 \\ \cos(7.5°) & 4\cos(15°) & 9\cos(22.5°) & 25\cos(37.5°) & 49\cos(52.5°) & 1 \\ \cos(15°) & 4\cos(30°) & 9\cos(45°) & 25\cos(75°) & 49\cos(105°) & 1 \\ \cos(22.5°) & 4\cos(45°) & 9\cos(67.5°) & 25\cos(112.5°) & 49\cos(157.5°) & 1 \\ \vdots & \vdots & \vdots & \vdots & \vdots & \vdots \\ \cos(352.5°) & 4\cos(705°) & 9\cos(1057.5°) & 25\cos(1762.5°) & 49\cos(2467.5°) & 1 \end{bmatrix} \end{array} \tag{29}$$

Different from the longitudinal displacement, the GBT transversal ones are not in the global membrane's coordinate system. Thereby, it requires the transformation given in eq. 24, which leads to:

$$[T_c]_{vw} = \begin{array}{c} \\ 529 \\ \vdots \\ 576 \\ 817 \\ \vdots \\ 864 \end{array} \begin{array}{c} \begin{array}{ccccccc} 529 & \ldots & 576 & 817 & \ldots & 864 \end{array} \\ \begin{bmatrix} -\sin(0°) & \ldots & 0 & \cos(0°) & \ldots & 0 \\ \vdots & \ddots & \vdots & \vdots & \ddots & \vdots \\ 0 & \ldots & -\sin(352.5°) & 0 & \ldots & \cos(352.5°) \\ \cos(0°) & \ldots & 0 & \sin(0°) & \ldots & 0 \\ \vdots & \ddots & \vdots & \vdots & \ddots & \vdots \\ 0 & \ldots & \cos(352.5°) & 0 & \ldots & \sin(352.5°) \end{bmatrix} \end{array} \begin{bmatrix} [T_c]_v \\ [T_c]_w \end{bmatrix} \tag{30}$$

4.2. Finite element solution

Once the multi-freedom constraint transformation matrices are evaluated for each displacement direction, a total form of these matrices, $[T_c]_{tot}$, can be built up.

As mentioned before, initially an identity matrix, I, is defined. Its dimensions have the same number of no-support degrees of freedom, 756x756. From this matrix, all columns corresponding to slave degrees of freedom are removed, which leads to the dimension 756x612. Thereafter, each component of the rows, which are concerning the slave degrees of freedom, is replaced by the respective term from the matrices $[T_c]_u$ and $[T_c]_{vw}$.

With the definition of the total multi-freedom constraint transformation matrix, one can achieve the coupled free stiffness matrix, $[K]_{cp}$ by eq. 25, in which the dimensions are 612x612.

Since in this example there is no external load applied in the slave degrees of freedom, the external load vector can be directly assembled without the related rows. Alternatively, one can apply eq. 26. The same external load vector is reached.

Finally, the numerical values of the degrees of freedom are achieved by a standard solver, such as the Cholesky decomposition, which is used here. Table. 3 presents the numerical solution for GBT elements:

Table 3: Solution of GBT's degrees of freedom, in mm

mode	$V\left(x=-\frac{L}{2}\right)$	$V_{,x}\left(x=-\frac{L}{2}\right)$	$V\left(x=0\right)$	$V_{,x}\left(x=0\right)$	$V\left(x=\frac{L}{2}\right)$	$V_{,x}\left(x=\frac{L}{2}\right)$
3	1.793E-1	5.535E-4	2.901E+2	1.298E-2	1.024E+2	1.116E-2
5	-1.302E-2	-4.488E-5	-1.325E+1	-4.788E-4	-5.867E+0	-5.130E-4
7	6.048E-4	2.088E-6	2.753E-1	9.021E-6	1.383E-1	9.172E-6
11	-6.473E-6	-2.351E-8	-1.573E-3	-4.965E-8	-7.885E-4	-5.257E-8
axial	7.619E-15	-1.524E-8	-4.573E-4	-1.524E-8	-2.287E-4	-1.524E-8

One important remark is concerning the indirect coupling among the GBT's degrees of freedom of orthogonal modes. Unlike the GBT's linear analysis, which each model is solved completely isolated from the others, in the mixed model this is no longer possible. The multi-freedom constraint transformation matrices build this indirect coupling, which requires solving a relative large linear system.

4.3. Analysis of displacement field

To perform an evaluation of the results obtained in the mixed model above, four full shell element models are used as a control parameter, obtained from commercial ANSYS® software. The difference among these models is the type of interpolation function applied: linear (shell-63 and shell-181) or quadratic (shell-93 and shell-281). These elements are based on one of the following kinematic hypotheses: Kirchhoff-Love (shell-63 and shell-93) and Mindlin-Reissner (shell-181 and shell-281). All models have the same discretization, which has 100 elements in the cross-section, and 610 segments in the longitudinal direction. In total, each model has 61,000 elements, which leads to 366,600 and 1,099,200 degrees of freedom for the linear and quadratic element models, respectively.

The two figures below plot the comparison among all models for the transversal displacement at top cross-section. The modal displacement field of GBT is plotted as well.

Figure 5: Results of top cross-section: transversal displacement of mixed shell-GBT element model. The GBT solution is obtained by the summation at top point of all modal deformation factors. The solution achieved from the fully shell element models are also presented.

Here, the results of transversal displacements obtained from different fully shell element models are almost the same. As shown in table 4, the highest mean difference is 0.93%, which occurs between GBT and the model with shell type 281. Also, the standard deviation is on the same order: 0.94%. The best agreement of results happens between GBT and the shell-93 model, which has the mean difference and standard deviation of 0.62% and 0.07%, respectively.

Table 4: Mean differences, in %, and standard deviation (SD) of displacement field between GBT and shell element models at top point

element	u		v		w	
	diff.	SD	diff.	SD	diff.	SD
Shell-63	0.16%	0.34%	0.7%	0.12%	0.6%	0.3%
Shell-93	0.08%	0.24%	0.62%	0.07%	0.55%	0.18%
Shell-181	0.17%	0.17%	0.93%	0.94%	0.84%	0.86%
Shell-281	0.62%	0.07%	0.54%	0.19%	0%	0%

The diagrams of longitudinal displacements are plotted below as well. Similar to transversal displacements, the differences among the models are almost imperceptible. The highest value of the mean difference is 0.62%, which is between GBT and Shell element type 281.

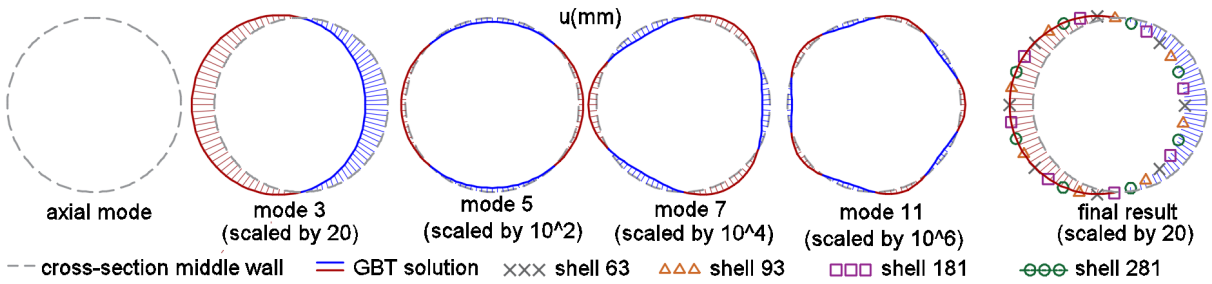

Figure 6: Comparison of results among mixed shell-GBT and fully shell models at top cross-section: longitudinal displacement.

4.4. Analysis of stress field

The comparisons among the mixed GBT-shell and the full-shell element models are placed at the longitudinal position of $x = 525mm$. This point leads to GBT domain in the mixed model and the center of the first elements after the coupling cross-section in the full-shell element models. For this cross-section, one can obtain the following internal bending moments:

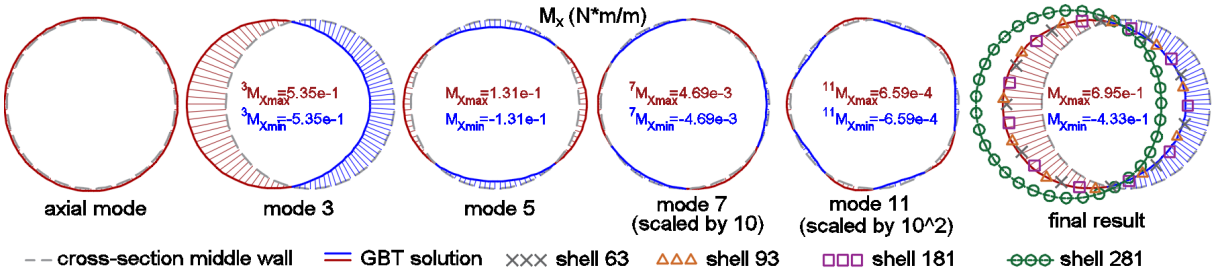

Figure 7: Comparison of results among mixed shell-GBT and fully shell models at point $x = 525mm$: longitudinal bending moment, M_x

Table 5 shows GBT approaches to the solution of Shell-93. Also, it indicates that there is no consensus among the different shell element models regarding the values of the plate's bending moment. Shell-281 has a clear deviation from the result of the other models.

Although Shell-93 gives the closest result to GBT in terms of the longitudinal bending moment, it provides the farthest one concerning the transversal bending moment, as shown in Table 6.

Concerning the twist bending moment, $M_{\theta x}$, GBT's results diverge from the Shell-93 ones and converge to those of other models. Similar to longitudinal bending moment, there is an increase

Table 5: Longitudinal bending moment, M_x, at $x = 525mm$: mean differences, (in the table's upper-right side), and their standard deviation (in the table's lower-left side) among all models

M_x	GBT	Shell-63	Shell-93	Shell-181	Shell-281
GBT	–	-9.22%	-0.59%	-9.45%	79.57%
Shell 63	2.09%	–	-8.57%	0.25%	95.65%
Shell 93	4.64%	2.3%	–	-8.8%	77.55%
Shell 181	2.07%	0.02%	2.31%	–	95.38%
Shell 281	19.48%	21.33%	22.18%	28.31%	–

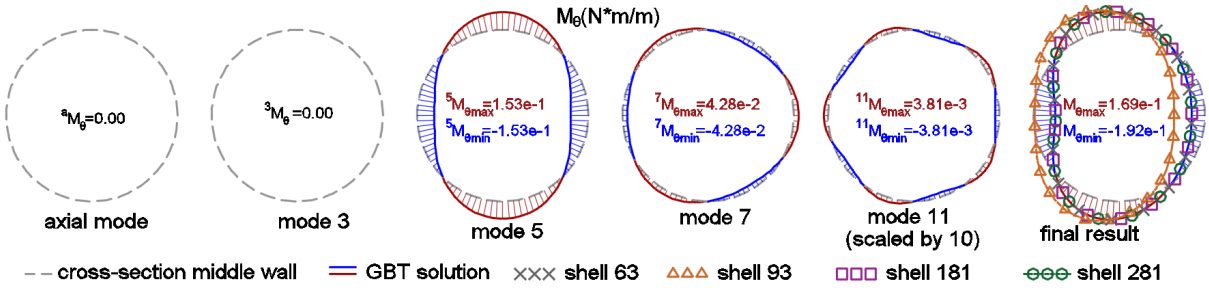

Figure 8: Comparison of results among mixed shell-GBT and fully shell models at point $x = 525mm$: transversal bending moment, M_θ.

Table 6: Transversal bending moment, M_θ, at $x = 525mm$: mean differences, (in the table's upper-right side), and their standard deviation (in the table's lower-left side) among all models

M_θ	GBT	Shell-63	Shell-93	Shell-181	Shell-281
GBT	–	0.52%	41.17%	0.59%	0.61%
Shell 63	0.48%	–	-77.16%	-0.06%	0.09%
Shell 93	192.69%	129.06%	–	-77.22%	-77.04%
Shell 181	0.89%	0.49%	131.32%	–	0.03%
Shell 281	0.29%	0.3%	128.97%	0.78%	–

in the mean difference among GBT and all shell models, simultaneously with a decrease in the standard deviation.

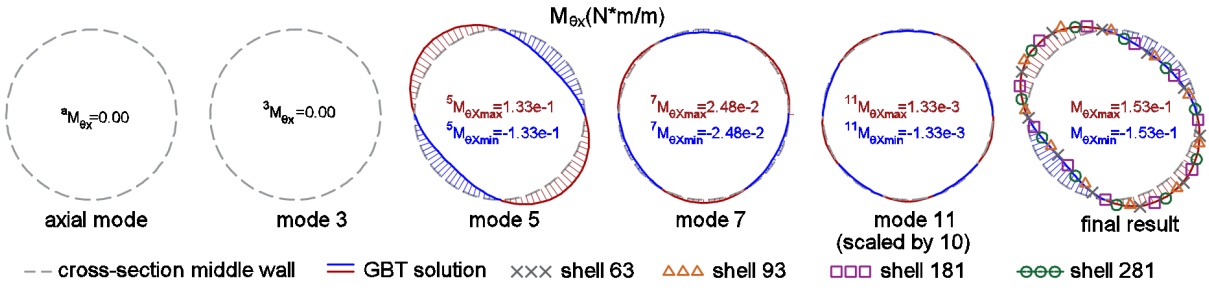

Figure 9: Comparison of results among mixed shell-GBT and fully shell models at point $x = 525mm$: twist moment, $M_{\theta x}$.

Following the same representation, the internal shear forces can be compared to the results from FEM based on shell elements, which indicates that GBT's longitudinal shear force, Q_x, approaches the results found for Shell-281. Shell-181 is another highlight in this internal force. As presented in figure 11, the results of this shell model not only show a quantitative difference, but also show a considerable qualitative one.

Table 7: Twist bending moment, $M_{\theta x}$, at $x = 525mm$: mean differences, (in the table's upper-right side), and their standard deviation (in the table's lower-left side) among all models

$M_{\theta x}$	GBT	Shell-63	Shell-93	Shell-181	Shell-281
GBT	–	6.7%	6.77%	6.08%	7%
Shell 63	5.1%	–	3.67%	1.07%	0.22%
Shell 93	18.41%	19.34%	–	1.1%	3.97%
Shell 181	6.05%	8.2%	11%	–	1.27%
Shell 281	6.35%	1.11%	20.39%	9.12%	–

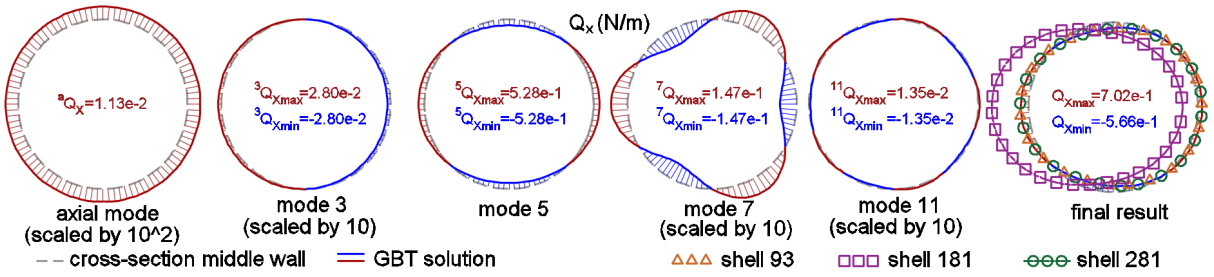

Figure 10: Comparison of results among mixed shell-GBT and fully shell models at point $x = 525mm$: longitudinal shear force, Q_x.

Table 8: Longitudinal plate's shear, Q_x, at $x = 525mm$: mean differences, (in the table's upper-right side), and their standard deviation (in the table's lower-left side) among all models

Q_x	GBT	Shell-93	Shell-181	Shell-281
GBT	–	7.29%	55.43%	7.21%
Shell 93	17.05%	–	-22%	1.34%
Shell 181	401.58%	544%	–	-69.95%
Shell 281	8.59%	10.1%	70.59%	–

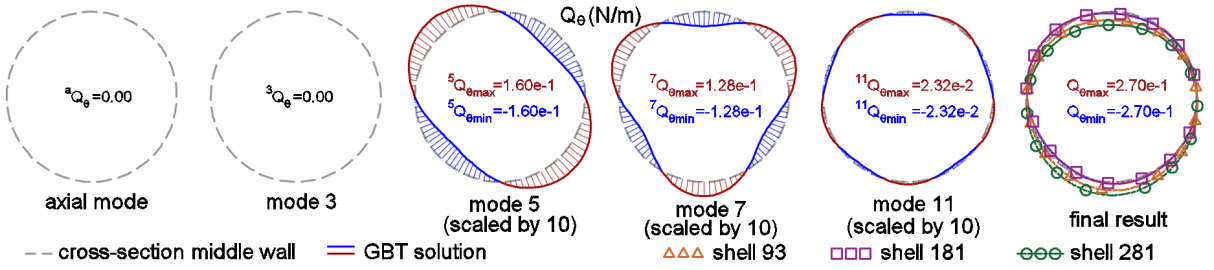

Figure 11: Comparison of results among mixed shell-GBT and fully shell models at point $x = 525mm$: transversal shear force, Q_θ.

On the other hand, in the analysis of transversal shear force, Shell-181 presents a lower difference from the GBT results, mean difference of 1.91% and a standard deviation of 6.67%.

The lack of consensus about the plate's internal forces does not happen in the case of longitudinal and shear membrane forces. The proposed GBT-shell coupling model and all shell models lead almost to the same solution. Each internal force is compared to the result of the shell finite element models in the cross-section at point x=525 mm, as well:

However, the approximation of the cross-section analysis to the support conditions is reflected

Table 9: Transversal plate's shear, Q_θ, at $x = 525mm$: mean differences, (in the table's upper-right side), and their standard deviation (in the table's lower-left side) among all models

Q_θ	GBT	Shell-93	Shell-181	Shell-281
GBT	–	73.27%	1.91%	23.34%
Shell 93	362.26%	–	-151.6%	87.48%
Shell 181	6.67%	87.84%	–	247.31%
Shell 281	496.43%	51.87%	852.02%	–

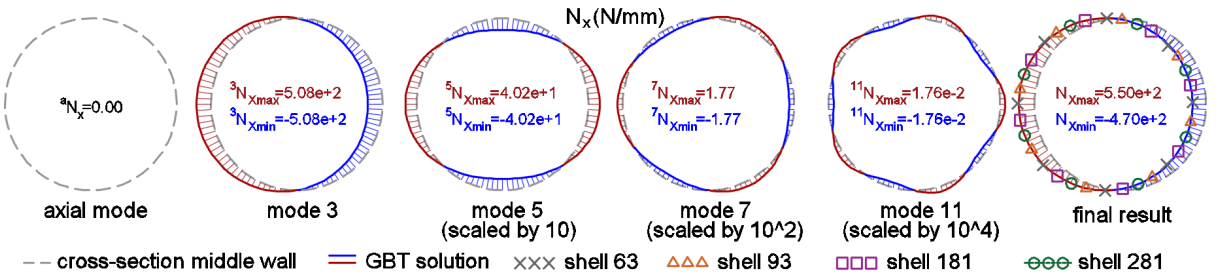

Figure 12: Comparison of results among mixed shell-GBT and fully shell models at point $x = 525mm$: longitudinal membrane force, N_x.

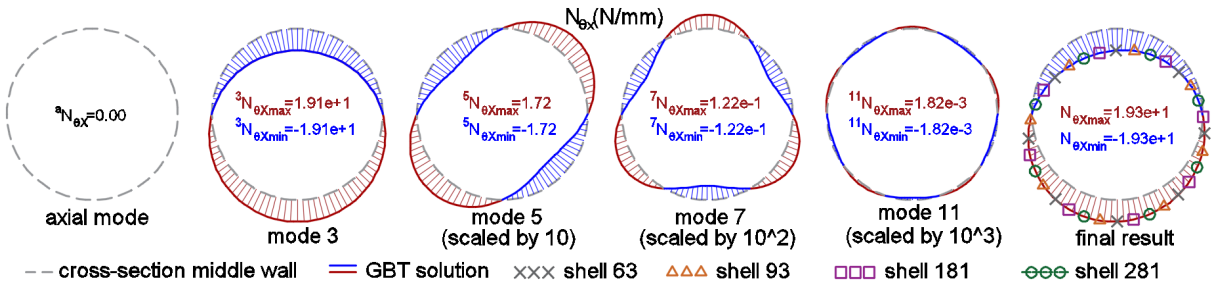

Figure 13: Comparison of results among mixed shell-GBT and fully shell models at point $x = 525mm$: shear membrane force, $N_{\theta x}$.

Table 10: Longitudinal membrane force, N_x, at $x = 525mm$: mean differences, (in the table's upper-right side), and their standard deviation (in the table's lower-left side) among all models

N_x	GBT	Shell-63	Shell-93	Shell-181	Shell-281
GBT	–	0.02%	-0.03%	0.05%	-0.03%
Shell 63	0.17%	–	0.05%	-0.03%	-0.05%
Shell 93	0.13%	0.04%	–	0.08%	0.01%
Shell 181	0.19%	0.02%	0.06%	–	-0.08%
Shell 281	0.13%	0.04%	0%	0.06%	–

in the membrane's result in transversal direction, N_θ: Shell-181 presents higher results than any other model. Moreover, there is no consensus among all models on the values of this internal force. Nevertheless, one can note that the values presented in figure 14 are really small compared to the values of the other membrane forces given in figures 12 and 13.

5. CONCLUSION

This study presents and evaluates a coupling approach between shell and GBT elements. The Multi-Freedom Constrain is based on the Master-Slaver method, from which the GBT degrees of freedom are set as Master ones. Thus, the coupling equations of this approach are based on

Table 11: Shear membrane force, $N_{\theta x}$, at $x = 525mm$: mean differences, (in the table's upper-right side), and their standard deviation (in the table's lower-left side) among all models

$N_{\theta x}$	GBT	Shell-63	Shell-93	Shell-181	Shell-281
GBT	–	0.02%	-0.01%	0.02%	-0.01%
Shell 63	0.15%	–	0.03%	0.01%	-0.03%
Shell 93	0.12%	0.03%	–	0.03%	0%
Shell 181	0.17%	0.02%	0.05%	–	-0.03%
Shell 281	0.13%	0.02%	0.01%	0.04%	–

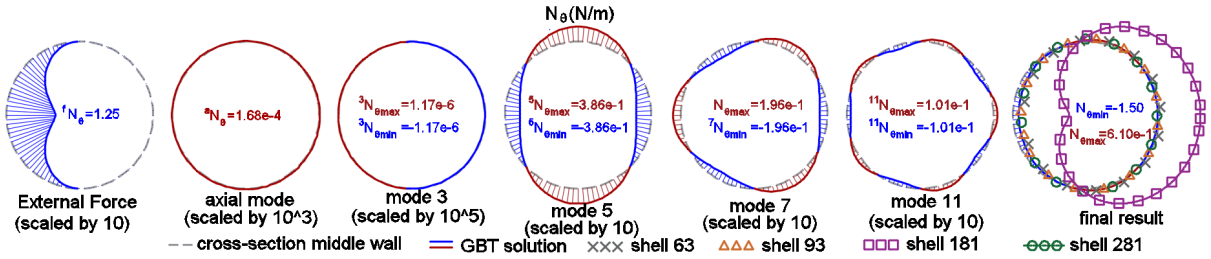

Figure 14: Comparison of results among mixed shell-GBT and fully shell models at point $x = 525mm$: transversal membrane force, N_θ

Table 12: Membrane tangential force, N_θ, at $x = 525mm$: mean differences, (in the table's upper-right side), and their standard deviation (in the table's lower-left side) among all models

N_θ	GBT	Shell-63	Shell-93	Shell-181	Shell-281
GBT	–	39.35%	22.54%	862.3%	35.73%
Shell 63	137.35%	–	14.87%	-82.61%	-82.2%
Shell 93	33.48%	115.82%	–	320.36%	26.09%
Shell 181	3.25%	0.87%	2041.77%	–	-86.47%
Shell 281	36.05%	110.91%	64.73%	0.79%	–

the modal displacements of GBT.

Two consequences are derived from these coupling equations: i) the coupling among GBT modes are already in the linear analysis; ii) the displacement and stress field of shell elements, in the neighborhood of the connection, are limited to GBT's assumptions.

Despite this limitation in shell elements, the numerical example shows a high convergence in the displacement field among the proposed mixed model and different types of full shell element models: i) linear or quadratic interpolation function; ii) Kirchhoff-Love or Mindlin-Reissner hypothesis.

Concerning the stress fields, it has imperceptible differences for the internal forces N_x and $N_{\theta x}$. The same evaluation can be built for the plate's bending moments M_x, M_θ and $M_{\theta x}$ and longitudinal shear force, Q_x. However, for these internal forces, one model of fully shell elements leads to divergent results. The GBT results are approximately the same as the other models' results.

The transversal shear force and the transversal membrane force, Q_θ and N_θ respectively, cannot have a conclusion of the perturbation of the coupling procedure, since all models have no consensus on the final results. Nevertheless, the results of these internal forces are much lower than any other internal force. In fact, they have a residual participation in the total stress field.

6. ACKNOWLEDGE

This work was carried out with support of CNPq (Conselho Nacional de Desenvolvimento Cientifico e Tecnologico - National Council for Scientific and Technological Development) - Brazil and Horizon 2020 MSCA-RISE-2015 project No. 691213 entitled “Exchange Risk”.

REFERENCES

[1] Richardt Schardt. *Verllgemeinerte Technische Biegetheorie*. Springer-Vertrag, 1989.

[2] Richardt Schardt. Generalized beam theory - an adequate method of coupled stability problems. *Thin-Walled Structures*, 19:161–180, 1994.

[3] Richardt Schardt. Lateral torsional and distortional buckling of channel-and hat-sections. *Journal of Constructional Steel Research*, 31:243–265, 1994.

[4] Leach.P Heiny D. Davies, J.M. Second-order generalised beam theory. *Journal of Constructional Steel Research*, 31:221–241, 1994.

[5] V.Z. Vlasov. *Thin-Walled Elastic Beams*. Israel Program for Scientific Translations, 1961.

[6] Camotim D. Silvestre, N. Influence of shear deformation on the local and global buckling behaviour of composite thin-walled members. In J. Loughlan, editor, *Proceedings of the 4th International Conference on Thin-Walled Structures*, pages 659–668. IOP Publishing Ltd, 2003.

[7] Camotim D. Silvestre, N. A shear deformable generalized beam theory for the analysis of thin-walled composite members. *Journal of Engineering Mechanics*, 139:Issue 8, 2012.

[8] Guitiérrez A. Miletta R. Miranda, S. and F. Ubertini. A generalized beam theory with shear deformation. *Thin-Walled Structures*, 67:88–100, 2013.

[9] Fujii D. Fujitani, Y. A structural analysis method of framed structures with thin-walled open section members based on the bending-torsional theory of beams. 61:749–763, 1998.

[10] Yan X.X. Zhang L. Tong, G.S. Warping and bimoment transmissiion through diagonally stiffened beam-to-column joints. 61:749–763, 2005.

[11] Kraus M. Kindmann, R. *Steel Structures design using FEM*. Berlin: Ernst adn Sohn, 2011.

[12] Camotim D. Silvestre N. Basaglia, C. Global buckling analysis of plane and space thin-walled frames in the context of gbt. 46:79–101, 2008.

[13] Camotim D. Silvestre N. Basaglia, C. Torsion warping transmission at thin-walled frame joints: Kinematics, modelling and structural response. 69:39–53, 2012.

[14] Crisfield M.A. Jelenic, G. Non-linear ‘master-slave’ relationships for joints in 3-d beams with large rotations. *Computer methods in applied mechanics and engineering*, 135:211–228, 1996.

[15] Crisfield M.A. Jelenic, G. Master-slave approach for the modelling of joints with dependent degrees of freedom in flexible mechanisms. *Communications in Numerical Methods in engineering*, 19:689–702, 2003.

[16] Habtemariam A. Bianco, M. and C. Koenke. Exact stiffness matrix in generalized beam theory. In B.W.Schafer and D.Ayhan, editors, *Proceedings of the 7th International Conference on Coupled Instabilities in Metal Structures*, pages 40.1–40.18. CIMS, 2016.

[17] KJ. Bathe. *Finite Element Procedures*. Prentice-Hall, 1996.